Distributed Magnetic Equivalent Circuit Modelling of Synchronous Machines

Oğuz Korman, Mauro Di Nardo, Jacopo Riccio, Mukhammed Murataliyev, Michele Degano, Chris Gerada

***Abstract*—This paper proposes a highly accurate and computationally efficient distributed magnetic equivalent circuit (DMEC) model for synchronous electric machines. The model - based on a two directional flux paths cell element - is derived in a general fashion in order to easily define different geometries. All the steps required for the DMEC definition and its nonlinear resolution are detailed including the rationals behind the geometrical discretization, the setting of the excitations and the boundary conditions implementation. A comprehensive comparison between results obtained using DMEC and FEM is provided for three different machine types, namely surface permanent magnet (SPM) machine, permanent magnet synchronous reluctance machine (PMaSynRel) and a synchronous reluctance (SynRel) machine in a wide range of operation points. The computational advantage of proposed model is also investigated as function of the level of discretization and so accuracy of the estimated performance. The predictions of the proposed DMEC model are fully experimentally validated with an extensive test campaign on an off-the-shelf synchronous reluctance motor.**

***Index Terms*—Distributed magnetic equivalent circuit, magnetic equivalent circuit, non-parametric equivalent magnetic circuit, synchronous reluctance, surface permanent magnet, permanent magnet assisted.**

I. Introduction

DESIGNING electric machines is a complex and nonlinear problem where the primary design tool is usually the finite element method (FEM) in the absence of an accurate and easy to implement analytical model. Although the accuracy of the FEM is high, its adoption within comprehensive design processes is hindered by its high computational burden. The latter is further exacerbated when more than one operating point needs to be optimized as in traction applications. Indeed, in such cases the performance estimation requires the complete knowledge of the machine magnetic and losses model, i.e. their dependency's with torque and speed.

History of analytical models based on simplified magnetic equivalent circuits dates back almost a century ago [1]. One of the first works [2] depicts magnetic equivalent circuits for transformers, induction machines (IM) and a salient-pole synchronous machines. IMs have been the main focus for MECs research since the beginning of the electrical machine history [3], [4]. Basically all kind of machines have been modelled using magnetic equivalent circuits as summarized in Table I.

O. Korman, J. Riccio, M. Murataliyev, M. Degano and C. Gerada are with the Power Electronics, Machines and Control Group, University of Nottingham, Nottingham, NG7 2GT, UK. (e-mail: oguz.korman@nottingham.ac.uk

M. Di Nardo is with the Department of Electrical Engineering and Information Technology, Politecnico di Bari, Bari, 70126, Italy (e-mail: mauro.dinardo@poliba.it)

The MEC models mentioned so far focus on specific machine types. Although they are quite valuable in terms of providing a comprehensive knowledge, the magnetic equivalent circuit is specific for a given machine as it represents its main flux paths. When dealing with anisotropic synchronous machines which feature a different behaviour according to the relative position between the rotor and the stator magneto motive force, two different modeling approaches have been proposed. The first one makes use of two distinct MECs able to represent the most important operating points, namely the direct and quadrature current supply conditions [18]. Although effective, this approach - even when implemented in a nonlinear fashion - does not allow to model the cross saturation phenomena, typical of anisotropic synchronous machine [19]. The other approach is to have only one MEC able to capture the magnetic behaviour in all supply conditions [20]. However, the topology of the rotor part of the MEC, which reflects the selected degree of the flux paths discretization, plays a major role in the realistic modeling of the cross-saturation. In general, the accuracy of the model increases with the number of nodes in the rotor equivalent circuit.

When the discretization level of the flux paths becomes independent from the underlying geometry, the modelling approach is called non-parametric, or finite reluctance or reluctance mesh-based. Hereafter, this approach will be refereed to distributed magnetic equivalent circuit (DMEC). This approach - focus of this paper - allows obtaining an overall excellent estimation of the magnetic fields within the machine with a much reduced computational burden compared with the FE approach. One of the first examples proposing this approach has been presented in [21], where the geometry is discretized into cells in a similar fashion like mesh is used in FEM. One of the most important aspects of this kind of MEC modelling is the ability to analyze various type of machines without changing the underlying definitions. Similar concepts has later been used to analyze axial flux

TABLE I: Overview of the literature on MEC

Machine Type	Reference
Induction Machine	[5] [3] [4]
Salient Pole Synchronous Machine	[6]
Stepper Motor	[7]
Linear Motor	[8] [9]
SPM motors	[10] [11]
Switched reluctance machines	[12]
Internal Permanent magnet Machine	[13] [14] [15]
Flux Switching Machines	[16]
Axial Flux Machines	[17]

This article has been accepted for publication in IEEE Transactions on Industry Applications. This is the author's version which has not been fully edited and content may change prior to final publication. Citation information: DOI 10.1109/TIA.2024.3462898

machines [22], switched reluctance machines [23] and flux switching machines [24]. In [25] IMs are modelled using a DMEC coupled with an electrical circuit and the performance estimations are compared with experimental results.

Along with the low computational cost and the outstanding accuracy, this magnetic modeling approach also allows to estimate the time-dependency of both electric and magnetic variables if the rotation of the rotor circuit part is implemented. All these advantages make this modeling approach the most suitable if a generic synchronous machine (i.e. with whatever rotor topology) has to be quickly analysed in different operating points or needs to be optimized.

Although this modelling technique has been already presented focusing on a given machine topology, a general framework able to analyse any synchronous machine is still missing along with the exploration of its limitation. This work - based on [26] - intends to fill this gap by providing a comprehensive approach to build a distributed magnetic model for any synchronous machine. Indeed, a novel and easy to implement definition of the magneto-motive force is introduced with this aim along with the inclusion of the magnetic periodicity and a generalised definition of the material distribution which all play a key role in defining the performance of the modelling approach. The aim is to build the basis for an alternative technique competitive to FEM in terms of accuracy and computation time. The paper is organized as follows. It starts with the description of all the steps required to build the model. Afterwards, the non-linear solution technique is described in detail. For the results part, three different machines, namely a surface mounted permanent magnet (SPM), a reluctance (SynRel) and its permanent magnet assisted version (PMaSynRel), are analyzed and compared with the FE estimation in terms of flux density distribution, torque waveform and average torque and torque ripple map in the d-q current plane. The effect of different level of discretization is also assessed with a sensitivity analysis to show the dependency of the performance accuracy with the computation time. As a vessel to verify the performance estimation approach, an off-the-shelf SynRel machine is tested in the full operating range confirming the validity of the proposed approach.

II. Description of the DMEC

The building block of a DMEC is a cell element (CE) and it consists of two horizontal and two vertical reluctances. A typical cell element is shown in Fig. 1 encircled with dashed red border. Although the reluctances and the cells are shown in cartesian coordinates, the modelling is developed in cylindrical coordinates and for this reason such reluctances will be referred as radial and tangential ones. A simple MEC consisting of 3 radial and 3 tangential CEs is shown in Fig. 1. Indexes of the CEs refer to their vertical position (i) and their horizontal position (j) respectivly. All CEs are connected with their adiajent neighbours allowing to model bi-directional flux flow in radial and tangential directions.

The selected solution technique is the loop (mesh) current method and the main unknown variable is the loop fluxes (Φ_L) as shown with red arrowed-circle in Fig.1. The main input

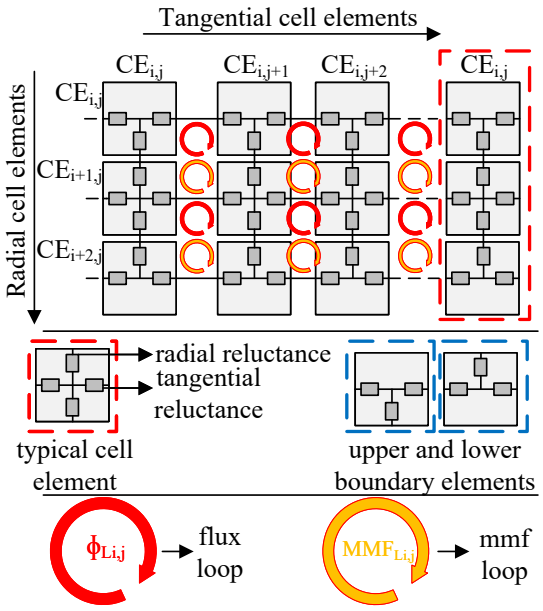

Fig. 1: Structure of the MEC and different CEs.

variables are the magnetomotive force loops (MMF_L) and reluctances (R). The number of total loops (n_L) can be written in terms of number of radial and tangential CEs (n_R, n_T) as $(n_R-1)\cdot n_T$. Likewise, the total number of reluctance elements n_{re} is $(2n_R-2)\cdot n_T + 2\cdot n_T \cdot n_R$.

A. Boundary conditions

Similar to FEM, boundary conditions should be considered in the DMEC modeling. In order to account for the zero flux condition (Dirichlet boundary), lower and upper CEs are structurally different than the middle CEs as shown with dashed blue border in Fig.1. The periodic boundary condition is implemented connecting the first and last column of CEs as shown in Fig. 1 where the first column of CEs are drawn also on the rightmost side of the DMEC with dashed red bounding box. Whether it is an even periodicity (e.g considering a pole pair) or an odd periodicity (e.g considering a single pole) this connection must exist. Difference between the odd and even periodicity conditions will be detailed in section III.

B. Discretization of the machine geometry

The number of CEs defines how fine the geometry is discretized. The selection of number of tangential n_T and radial cell n_R should be done considering the tradeoff between model complexity (i.e. matrix size) and its accuracy in predicting the performance. Once the number of CEs are defined, the material of each cell is defined by identifying the material at the centroid of the considered cell. By doing so a material matrix (M) for each constituent material can be built made of 0 and 1.

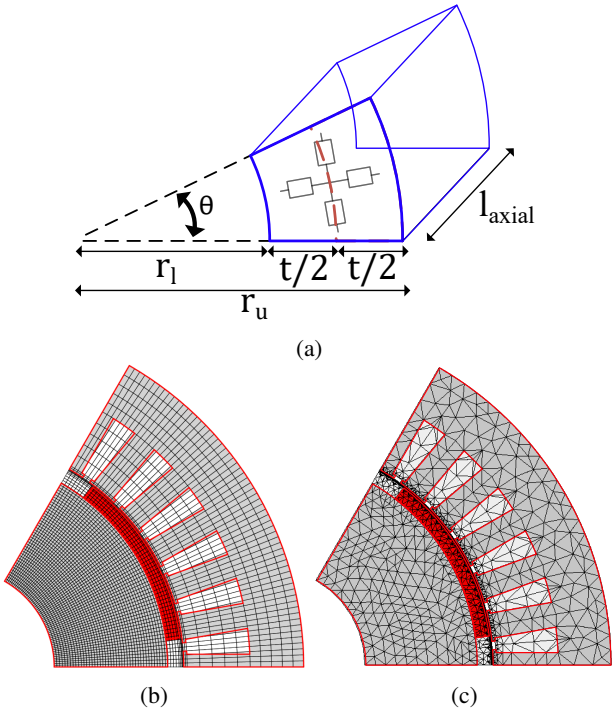

(a) (b) (c)

Fig. 2: a) CE and reluctance dimensions b) SynRel machine geometry DMEC mesh b) SynRel machine geometry FEM mesh .

Fig. 2b shows discretization of a parallel tooth stator with a three-barrier SyRel rotor with 60 tangential and 63 radial CEs. Obviously, a perfect representation of the target geometry cannot be achieved due to the shape of CEs being arc segments. However, a good representation is possible if the size of the CEs is selected according to the CE position within the geometry. For example in Fig.2b, the size of the CEs for rotor tangential ribs and stator tooth tip is smaller than all the other in order to be able to capture all the magnetic flux paths.

C. Handling the rotation

Rotating structures can also be defined by applying a simple update scheme to M. Since the rotating part of the geometry and M is known, for each rotation step some part of M is shifted. Using this method, it is possible to apply rotation without changing the connection and/or index of the cells which is an obvious advantage. However, the maximum number of rotation steps are limited to the number of tangential cells.

D. Calculation of the reluctance

A reluctance can be expressed as function of the length of the reluctance path (l), area where flux crosses (A) and material dependent reluctivity $\upsilon(B)$. Given the high number of cells, the following relationship can be used (1):

$$R = \frac{l}{A}\upsilon \tag{1}$$

The length and area of radial reluctances (see Fig. 2a) can be then defined using the equations (2) (3) (4) in which l_r, A_{lr} and A_{ur} stands for length of the radial reluctance, area of the lower side radial reluctance and area of the upper side radial reluctance respectively while the axial length of the system is denoted with l_{axial}.

$$l_r = \frac{t}{2} \tag{2}$$

$$A_{lr} = \frac{2\pi}{360}\ (r_l + \frac{t}{4})\ \theta\ l_{axial} \tag{3}$$

$$A_{ur} = \frac{2\pi}{360}\ (r_l + \frac{3t}{4})\ \theta\ l_{axial} \tag{4}$$

Similarly for the tangential reluctances, dimensions can be written as in (5) and (6). Here l_t and A_t are the length and area of the tangential reluctances.

$$l_t = \frac{\pi}{360}\ (r_l + \frac{t}{2})\ \theta \tag{5}$$

$$A_t = t\ l_{axial} \tag{6}$$

E. MMF definition

MMF sources, i.e. permanent magnets and winding system, can be expressed as voltage sources in the DMEC. In this work, a slightly different approach is adapted. Instead of placing voltage sources in the branches of the equivalent circuit, loop quantities are used to reflect MMF directly as loop sources.

Once the MMF from windings and PMs are known, they can be expressed as a single MMF matrix as $MMF = MMF_W + MMF_{PM}$. Such MMF matrix is obviously function of time (MMF_W) and rotor position (MMF_{PM}).

MMF of the winding (MMF_W) can be expressed as in (7) where N is the number of turns and I is the current:

$$MMF_W = \oint H\,dl = N \cdot I \tag{7}$$

MMF of a single coil CE is equally distributed among its neighbouring four loops where each loop contributes for $\frac{NI}{4}$. When the winding area is made of more than a single coil CE, the total number of turns have to be shared among the coil CEs with respect to their surface area to find individual CE's share. This can be calculated using (8):

$$MMF_{CE_{ij}} = \frac{MMF_W}{\sum SA_{CE_{ij}}} \cdot SA_{CE_{ij}} \tag{8}$$

After each coil CE's MMF is found, the MMF contribution from neighbour CEs has to be added together to find the aggregated MMF in the loops. An example case where 2 coil CEs exist with the same surface area is illustrated in Fig. 3.

In the case of the PM excitation, MMF is again reflected between the CE's four shared loops in an unequal way to account for magnetization direction. An example model consisting of a single PM CE is shown in Fig. 3. The neighbouring loops

are numbered from MMF_{PM-1} to MMF_{PM-4} and can be calculated as:

$$\begin{aligned} MMF_{PM-1} &= \frac{1}{2}[+H_c l_t cos(\alpha) + H_c l_r sin(\alpha)] \\ MMF_{PM-2} &= \frac{1}{2}[+H_c l_t cos(\alpha) - H_c l_r sin(\alpha)] \\ MMF_{PM-3} &= \frac{1}{2}[-H_c l_t cos(\alpha) - H_c l_r sin(\alpha)] \\ MMF_{PM-4} &= \frac{1}{2}[-H_c l_t cos(\alpha) + H_c l_r sin(\alpha)] \end{aligned} \tag{9}$$

In (9), H_c is the coercivitiy of the magnet, l_t and l_r are tangential and radial lengths of the corresponding cell elements while α is the magnetization direction. It is worth noting that, if the dimensions of the reluctances are calculated in cylindrical coordinates as in this case, α has to be calculated for each CE with respect to their centroid's location. For instance, in the cylindrical coordinates $\alpha = 90^o$ creates a radially magnetized magnet.

III. Solution Technique of the DMEC

Once the DMEC is build, it is solved with the loop method which identify the unknown loop flux vector ϕ_L knowing the loop mmf vector MMF_L and the loop reluctance matrix R_L. The matrix equation has to be solved iteratively to account for the nonlinear behaviour of ferromagnetic steel. Newton-Raphson method is employed for this purpose due to its good convergence characteristics [22], [23]:

$$r = R_L\,\phi_L - MMF_L \tag{10}$$

In (10) r is the residual and needs to be reduced as much as possible during the iterations. The loop reluctance matrix has a size of $[n_L \times n_L]$ and its elements reflect the reluctances in the

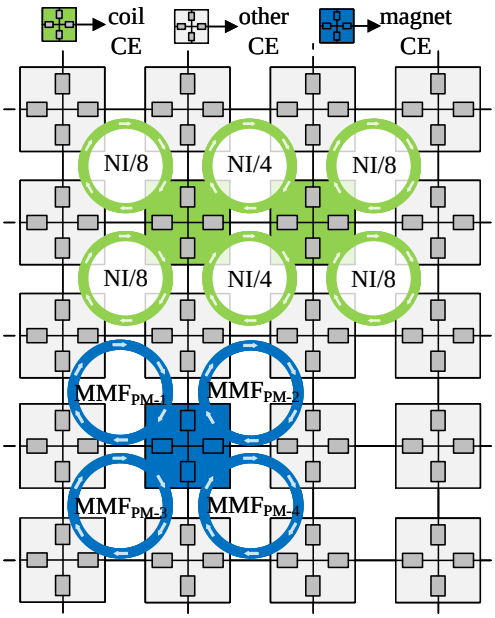

Fig. 3: Definition of MMF sources due to windings and PMs

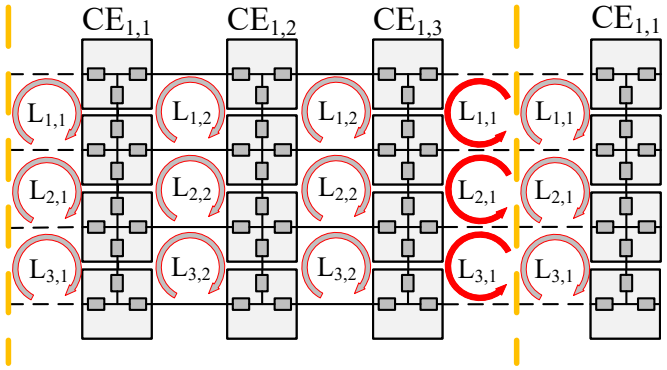

Fig. 4: Depiction of loop directions in the presence of odd periodicity conditions.

respective loop and the reluctances shared between different loops. ϕ_L and MMF_L are single column vectors of the size of $[n_L \times 1]$.

The loop reluctance matrix R_L can be calculated by using the diagonal reluctance matrix of all materials (R_{tot}) and the loop incidence matrix L as shown in (11):

$$R_L = L^T \mathbf{R_{tot}}\, L \tag{11}$$

The total diagonal reluctance matrix $\mathbf{R_{tot}}$ can be expressed as the sum of two diagonal matrixes: one containing the linear materials $\mathbf{R_{lin}}$ which can be expressed as:

$$\mathbf{R_{lin}} = \mathbf{R_{air}} + \mathbf{R_{PM}} + \mathbf{R_{copper}} \tag{12}$$

while the other one containing the non linear material, i.e. the iron. The latter can be expressed as the product between its the diagonal matrix of reluctances without the reluctivity terms ($\mathbf{R_{iron}}$) and the diagonal matrix of reluctivities ($\upsilon_\mathbf{r}$).

The incidence matrix L has a size of $[n_{re} \times n_L]$ and basically gives information about how each reluctance is associated with each loop. If a loop flux passes through a reluctance in the predefined direction it attains the value 1, if it passes in the opposite direction it becomes -1 while if they are not related it becomes 0. Using this information shared reluctances between different loops are identified.

Apart from that, L also determines the periodic boundary conditions. When an even boundary condition has to be imposed, L is built as just described. However, for an odd boundary conditions, the last loops (column-wise) has to be modified. This modification is illustrated in Fig. 4 where the part of the last loop facing the last reluctances in a row changes the direction in order to impose flux contributing from the unmodelled part of the system in an equal but opposite direction.

A. Nonlinear iteration

Using the Newton-Raphson scheme, ϕ_L is found iteratively until convergence. The flux vector at the $k+1$ step is given as:

$$\phi_L^{k+1} = \phi_L^k - J\,r^k \tag{13}$$

where the Jacobian matrix J provides the derivative of the flux with respect to material characteristics. The evaluation of the

Jacobian matrix is carried out with the approach presented in [22]:

$$J = R_L + L^T(\mathbf{R_{iron}} \cdot \mathbf{A}^{-1} \cdot \frac{d\boldsymbol{\upsilon_r}}{d|\boldsymbol{B}|})((L\,\boldsymbol{\phi_L}\,U) \cdot L) \quad (14)$$

Here A is the flux-crossing area of the reluctance elements (iron materials) in the diagonal form. $\frac{d\boldsymbol{\upsilon_r}}{\boldsymbol{d|B|}}$ is the derivative of reluctivity with respect to the absolute value of the flux density which can be found numerically by applying central differences formula in (15) ensuring a small perturbance (Δ_B):

$$\frac{d\boldsymbol{\upsilon_r}}{\boldsymbol{d|B|}} = \frac{(\boldsymbol{\upsilon_r}(|B|) + \Delta_B) - (\boldsymbol{\upsilon_r}(|B|) - \Delta_B)}{2\Delta_B} \quad (15)$$

$\boldsymbol{\phi_L}$ and $\boldsymbol{B}$ are loop fluxes and flux density of reluctance in the diagonal form. Finally, U is a matrix storing information about how flux loops are related. It can be found by replacing the nonzero elements with 1 in $L^T L$.

B. Calculation of electromagnetic quantities

Once all flux loops are computed, it is possible to calculate the flux densities of each reluctance. First, the flux passing through each reluctance ($\boldsymbol{\phi_{RE}}$) is found by using (16). After that, the flux density of each reluctance $\boldsymbol{B_{RE}}$ is found with (17). Here both ($\boldsymbol{\phi_{RE}}$) and $\boldsymbol{B_{RE}}$ are of size $[n_{RE} \times 1]$.

$$\boldsymbol{\phi_{RE}} = L\,\boldsymbol{\phi_L} \quad (16)$$

$$\boldsymbol{B_{RE}} = \boldsymbol{\phi_{RE}^T}\,\boldsymbol{A^{-1}} \quad (17)$$

Electromagnetic torque can be calculated by using Maxwell's stress tensor which in its discrete form is reported in (18)

$$T = \frac{2\pi}{n_T \mu_0} r^2 l_{axial} \sum B_{rad} \cdot B_{tan} \quad (18)$$

where μ_0 is the free space permeability, r is the airgap radius, B_{rad} is the radial flux density and B_{tan} is the tangential flux density.

Using (19), the flux linkages of each CE can be calculated as:

$$\lambda_{CE_{ij}} = \frac{SA_{CE_{ij}}}{4SA_W} \sum_{k=i-1}^{i} \sum_{l=1}^{j+1} \phi_{L_{kl}} \quad (19)$$

where SA_W is the total surface area of the winding while $\phi_{L_{kl}}$ are the loop fluxes surrounding the considered cell ij.

Flux linkage of a winding area λ_W can be written as the aggregated sum of all the respective λ_{CE_ij}. Now that flux linkages in a winding region, i.e stator slot, is known, the total flux linkage of the entire phase winding can be calculated using the winding matrix. For instance a single layer winding configuration for 36 slot 6 pole machine using odd pole symmetry (so 6 slots) can be written as:

$$\begin{array}{rcl} W_A &=& [1 \quad 0 \quad 0 \quad 0 \quad 0 \quad -1] \\ W_B &=& [0 \quad 0 \quad 0 \quad 1 \quad 1 \quad 0] \\ W_C &=& [0 \quad -1 \quad -1 \quad 0 \quad 0 \quad 0] \end{array} \quad (20)$$

Considering λ_W as a row vector, the phase flux linkage can be calculated using the equations below, where k_p stands for the periodicity (for 36 slot 6 pole odd periodicity k_p=6) and N_t is the number of turns in each slot:

$$\lambda_A = \lambda_W W_A^T \cdot k_p \cdot N_t \quad (21)$$

$$\lambda_B = \lambda_W W_B^T \cdot k_p \cdot N_t \quad (22)$$

$$\lambda_C = \lambda_W W_C^T \cdot k_p \cdot N_t \quad (23)$$

TABLE II: Specifications and dimensions of the SPM, SynRel and PMaSynRel machines.

General Dimensions		
Parameter	Value	Unit
Stator outer radius	123	mm
Rotor outer radius	80	mm
Air-gap length	0.7	mm
Shaft radius	35	mm
Stack length	120	mm
Rated current	82	A_{peak}
Current density	10	A_{RMS}/mm^2
Lamination material	M250-35A	
SPM Parameters		
Magnet thickness	5	mm
Magnet span	45	mech. deg. ^{o}
Magnet Material	N42EH	
SynRel Parameters		
No of barriers	3	
Radial ribs thickness	2	mm
Tangential ribs thickness	1	mm
PMaSynRel Parameters		
No of Barriers	3	mm
Magnet Thicknesses	3.01-6.84-12.18	mm
Radial ribs thickness	3	mm
Tangential ribs thickness	1	mm
Magnet Material	N42EH	

IV. Performance estimation and FE validation

Three different machines, a SynRel, an SPM and a PMaSynRel machine have been analyzed using the developed DMEC model and the results are compared with the respective FEAs. FEAs are conducted using Ansys Maxwell commercial software. All machines share the same stator (36 slots and 6 poles) and single layer winding configuration. The SPM machine has a radial magnet shape and perpendicular magnet orientation. SynRel and PMaSynRel machines have been created using Joukowski flux barriers [27]. Parametrization for the SynRel and PMaSynRel machines are based on a previous work presented in [28]. Detailed information about the machines in terms of dimensions, materials and other properties have been given in Table. II

Three different set of analysis will be shown in the following: the first one looks at one single operation point in terms of flux density distribution and torque waveform; the second one analyse the three machines in the entire dq current plane in terms of flux linkage, average torque and torque ripple. The last analysis aims to identify the tradeoff between accuracy of the estimated performance and computational time by varying the spatial discretization.

A. Single operating point

Number of CEs in radial and tangential direction are kept the same for the analysis of all three machines. The number

This article has been accepted for publication in IEEE Transactions on Industry Applications. This is the author's version which has not been fully edited and content may change prior to final publication. Citation information: DOI 10.1109/TIA.2024.3462898

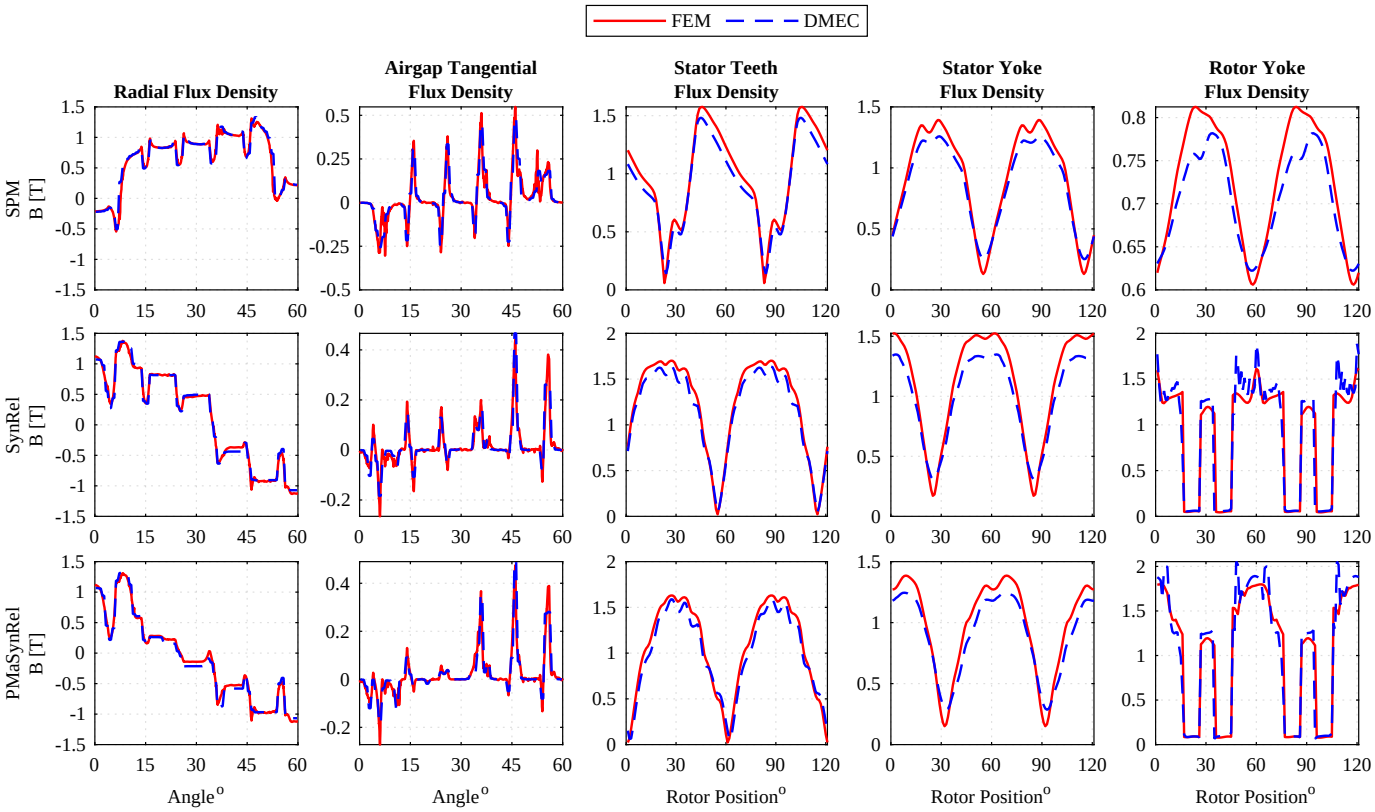

Fig. 5: Airgap flux density and flux densities in different regions of the machine as a function of rotor position.

of tangential CEs have been selected to be 60 in order to have 1^o resolution while in terms of radial CEs in the airgap and rotor these are fixed at 3 and 48 respectively while the stator to 12. The discretization for both DMEC and the FEM model are shown for the SPM machine as depicted in Fig. 2b and 2c.

Fig. 5 shows the airgap flux density distributions in terms of radial and tangential components for a given rotor position for all the three machines. The same figure also reports the flux density sampled in the middle of the tooth, stator yoke and rotor yoke as funtion of the rotor position. The comparison of the airgap flux density waveforms reveals an overall good match for all three machine types with some minor differences mainly in the airgap tangential component. Comparing the flux density variation with respect to the rotor position, it is seen that the waveform shape and trend are well matching despite the fact that MEC predicts slightly lower values. Fig. 6 shows the flux density distributions of the machines as obtained through DMEC and FEM. Examination of both distributions give very close match in terms of contour shapes and values. Very limited discrepancies can be seen in small saturated areas such as ribs and stator tooth tips.

The average torque, torque ripple and computation time are summarized in Table. III. Both FEA and analysis using DMEC has been done for a total of 21 equally divided time steps for one sixth of the electrical period. The average torque estimation is basically the same obtained with the FEA confirming the outstanding capability of the DMEC. On the

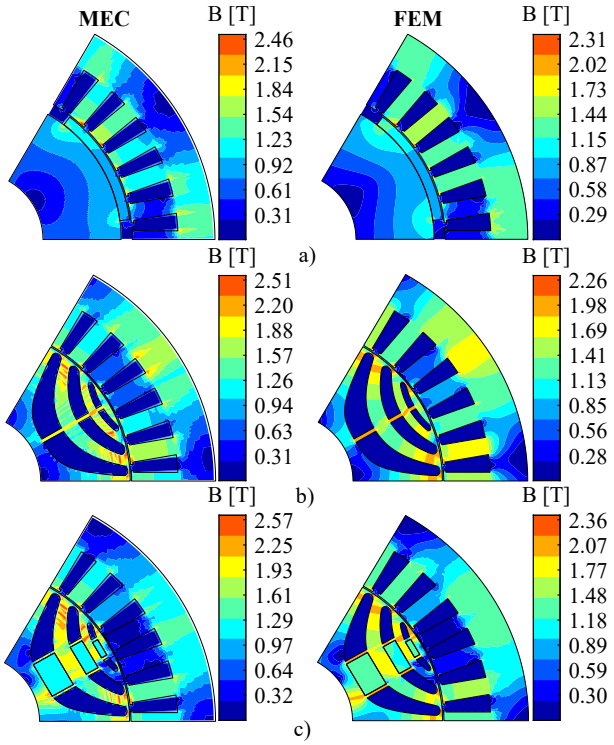

Fig. 6: Flux density distribution obtained with MEC (left column) and FEM (right column), a) SPM machine, b) SynRel machine, c) PMaSynRel machine.

TABLE III: Single point comparison of FEM and MEC

	SynRel		PMaSynRel		SPM	
	FEM	**MEC**	**FEM**	**MEC**	**FEM**	**MEC**
Mesh&CEs	4958	3780	4761	3780	3614	3780
Time [s]	46.4	3.8	52	4.1	47.9	2.4
Torque [Nm]	74.9	74.6	104.7	109.4	120.6	122.2
Ripple [%]	12.3	33.3	17.4	29.4	25.8	23

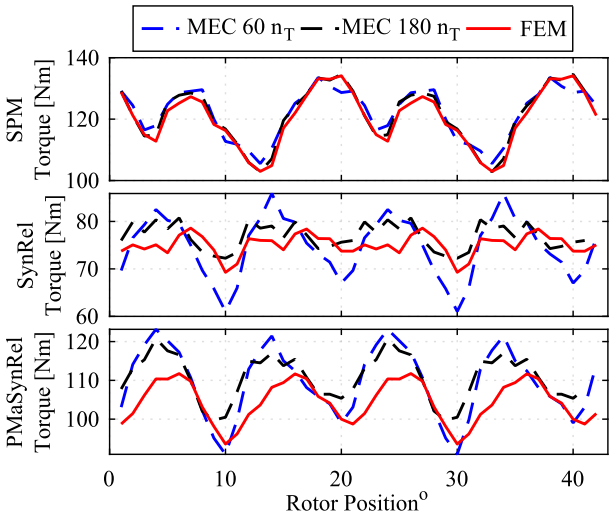

Fig. 7: Torque as function of the rotor position for the three considered machine topologies evaluated with the MEC and the FEA.

other hand, the estimated torque ripple differ from the FE one due to the inability to capture all the airgap harmonics with this considered amount of tangential CEs. Torque waveforms are reported in Fig. 7 for the analyzed case (60 tangential cells) and also when the tangential CEs are increased to 180. Analysing this figure, it is clear that the obtained waveforms are closer to the FE one when a more refined tangential discretization is adopted.

From computational point of view, the DMEC clearly provides a tremendous advantage in terms of computation time, being 12 to 20 times faster as summarized in Table III. It is worth to underline that the FEA have been performed with a number of mesh elements similar to the number of CEs in the DMEC in order to set a fair comparison from the computational point of view. Computation times of the DMEC models when the number of tangential CEs are increased to 180 (total CEs become 11340) as reported in Fig. 7 are 18.8s, 20.1s and 8.2s for SynRel, PMaSynRel and SPM machines respectively.

B. Analysis in the D-Q current plane

All machines are analyzed in a cartesian grid of the dq current plane up to double the rated current (160 A_{peak}) with equally spaced 100 grid points. For the discretization of machines the number of tangential CEs are increased to 120 to get a more accurate description of the geometry, especially small regions such as slot openings, magnet spans and end-point angles of the flux barriers. Analyses are again done for one sixth of the electrical period and 21 total steps. Results of these analysis are showed in Fig. 8 in terms of flux-current relationship, average torque and torque ripple contours.

The flux-current plot shows a good overall agreement for all machines both in terms of d and q-axis fluxes. Specifically the d-axis flux captured both by FEM and DMEC are in good agreement. There is negligible mismatch towards higher saturation areas where d-axis current is increasing which can be explained by imperfect geometry definiton. Considering the q-axis fluxes, very similar behaviours are obtained for the SPM and SynRel machines whereas there is a visible difference for the PMaSynRel machine. This is a direct consequence of discretization using CEs in polar coordinates. Indeed, a rectangular shaped PM cannot be perfectly represented with a polar discretization, which is reflected as an almost constant difference for the PMaSynRel machine. In spite of these differences, cross-coupling between d and q-axis fluxes are well captured.

The average torque contours directly reflect what can be seen in the flux-current plots. Indeed, the estimation error of the PM flux linkage causes an error in torque estimation of SPM and PMaSynRel machines. Nevertheless, it can be stated that estimated torque contour perfectly match the FE one. Average differences in the plane are 2.2%, 7.3% and 1.7% for SynRel, PMaSynRel and SPM machines respectively.

Considering the torque ripple performance, there is an overall good matching in terms of contour shapes and values for all machine types. Although there is a consistent match, prediction of torque ripple values are not as good as fluxes and average torques. These differences can be directly ascribed to the extremely high sensitivity of the torque ripple to the level of tangential discretization of the DMEC.

C. Sensitivity analysis

The goal of this section is to identify the sensitivity of the results obtained with the DMEC with respect to number of CEs. The PMaSynRel machine is selected for this analyses as it is the most challenging. Indeed, it presents the most complicated geometry, difficult to be represented in a discretized form and so more prone to lead to discrepancy between the DMEC estimation and the FE one.

A single operating point in deep saturation (I_q=17.78A and I_d=124.45A) is selected as it features the highest error torque error (see Fig. 8).

The sensitivity analysis are performed looking at average torque and torque ripple with respect to number of CEs in different part of the machine. In particular, four analysis have been carried out whose results are shown in Fig. 9:

- s_1: the number of radial CEs describing the rotor tangential ribs are increased;
- s_2: the number of radial CEs describing the rotor are changed but the ribs part stays constant (=2).
- s_3: the number of radial CEs describing the stator yoke and teeth parts are increased;
- s_4: the number of tangential CEs are increased. Number of tangential CEs are varied in multiples of 60 in order to always be able to simulate the same rotor positions (analyses are performed always with 21 steps).

This article has been accepted for publication in IEEE Transactions on Industry Applications. This is the author's version which has not been fully edited and content may change prior to final publication. Citation information: DOI 10.1109/TIA.2024.3462898

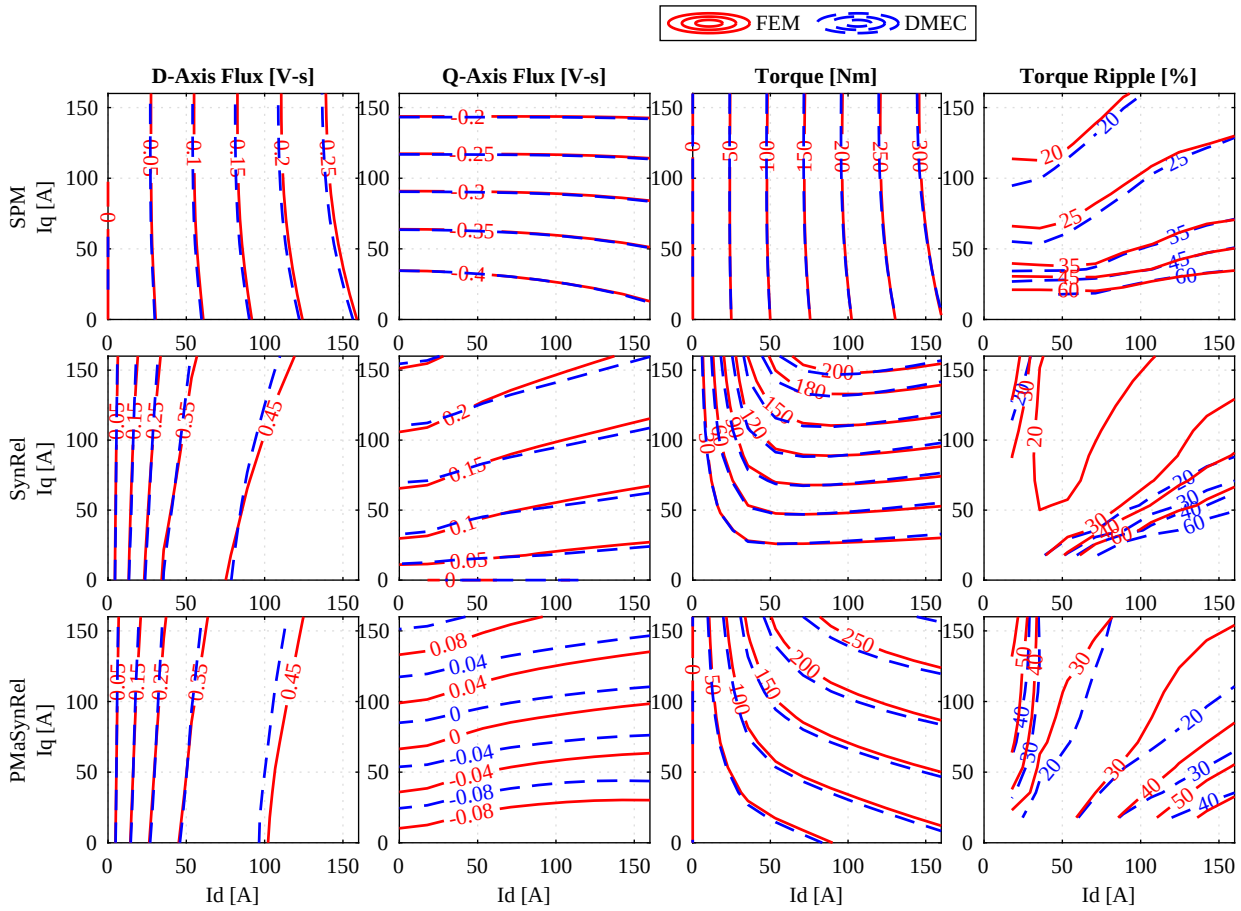

Fig. 8: Flux, torque and torque ripple contour maps with respect to d and q-axis currents for SynRel, PMaSynRel and SPM machines using FEM and DMEC.

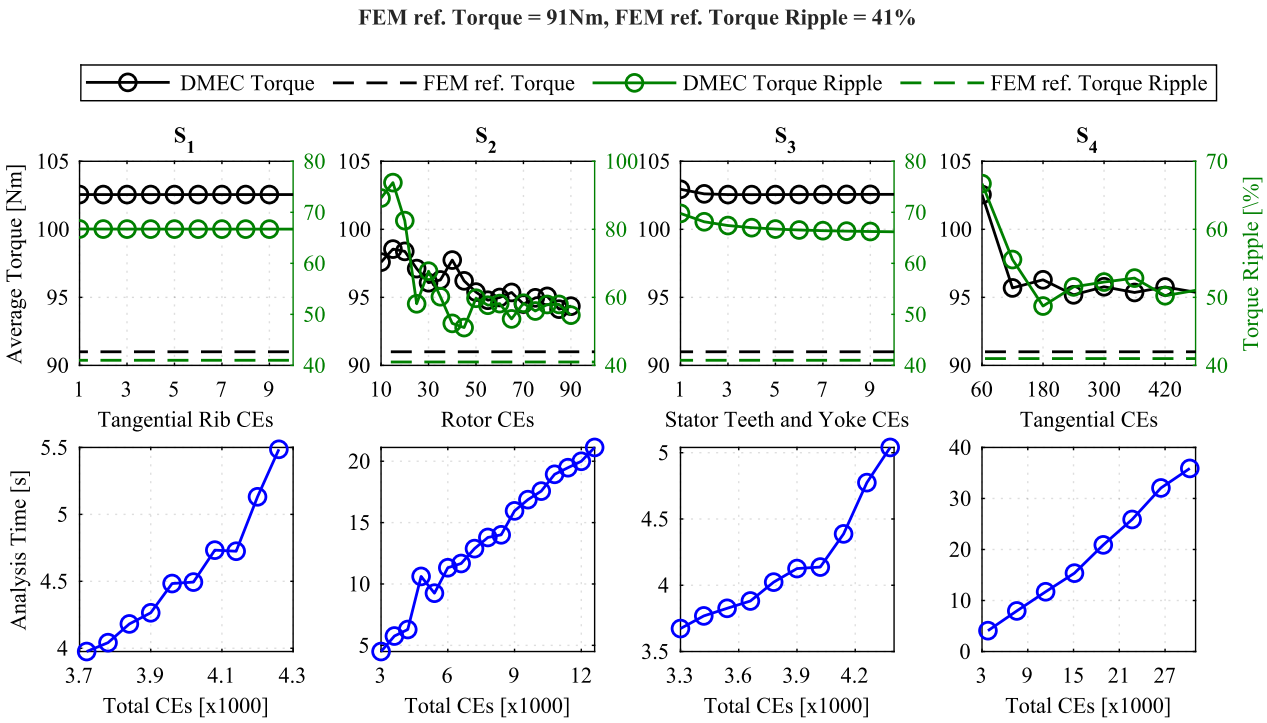

Fig. 9: Results of sensitivity analysis and corresponding computation times

The same figure also reports the computational time as function of the different number of CEs; the analysis have been performed on a workstation Intel Xeon W-2123 CPU @3.6 GHZ with 32GB RAM.

Regarding the first case (s_1), it is seen that increasing the number of radial CEs in the tangential ribs region has no effect on average torque or torque ripple.

For the second case (s_2), average torque and torque ripple values get closer to the reference values (FEM results always reported in Fig. 10). The spikes in the descending trend of both average torque and torque ripple can be ascribed to the fact that the material matrixes and so the modeled geometry changes with the discretization.

In the case of increased radial CEs describing the stator teeth and yoke regions (s_3), it can be deduced that increasing this parameter is beneficial up to a certain point above which does not lead to major benefit but just increases the computational time. On the other hand, the number of tangential CEs plays a more clear and critical role in defining the accuracy of the DMEC model, as shown in study s_4. In general, more the number of tangential CEs are used, better results can be obtained with a drawback of computational time.

It can be concluded that for rotating radial flux electric machines, where electromagnetic excitations are circumferentially distributed, the number of tangential cells plays a key role.

V. Experimental validation

An off-the-shelf SynRel machine is tested and the results are compared with both DMEC and FEA estimation. General specifications of the machine as well as dimensions are provided in Table IV. The experimental test bench is shown in Fig. 10. Both prime mover (permanent magnet machine) and machine under test are driven by two 2L-VSI sharing the same DC-link powered by a DC power supply. A custom control platform [29] is used to implement the control and identification algorithms.

A. Test procedure

The aim of the experiments is to obtain the characteristics of the machine under test in terms of flux-current and torque-current relationship. The magnetic model identification procedure presented in [30] has been adopted. With this methodology, d and q-axis fluxes are obtained through measuring and post-processing d and q-axis current and voltages while the machine under test is current controlled in motoring and generating mode and the prime mover is speed controlled.

TABLE IV: Specifications of the tested SynRel machine.

General Dimensions		
Parameter	Value	Unit
Statour outer radius	75	mm
Shaft radius	15	mm
Specifications		
Rated speed	1500	RPM
Rated power	1.1	kW
Rated current	4.1	A_{peak}

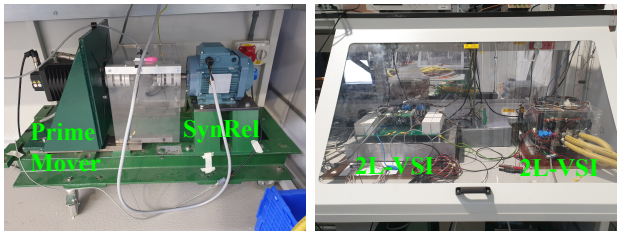

(a) (b)

Fig. 10: Test setup: a) SynRel and prime mover, b) control platform and inverter.

Specifically by following (24) and (25), it can be proved that the fluxes can be obtained without knowing the stator resistence:

$$\lambda_q = \frac{v_{qM} + v_{qG}}{2w} \tag{24}$$

$$\lambda_d = -\frac{v_{dM} + v_{dG}}{2w} \tag{25}$$

In (24) and (25), subscripts M and G refers to the motoring and generation modes, respectively. The currents required for these operations are complex conjugate vectors which lead to a complex conjugate flux linkage vectors as long as the iron losses are negligible. As a consequence, the speed during the tests is kept as low as noise to signal ratio of the measurement allows. Fig. 11 shows the reference and real current and voltage during the motoring and generating modes constituting the test required for the identification of one operating point. The same figure also report the averaging windows considered for the calculation. Once the fluxes are

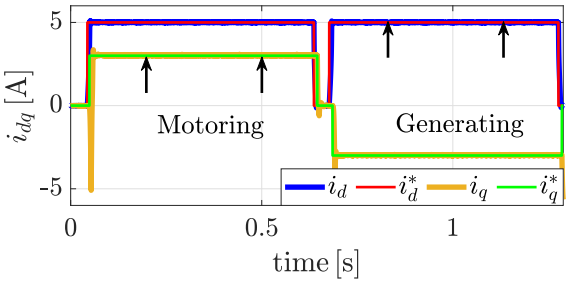

(a)

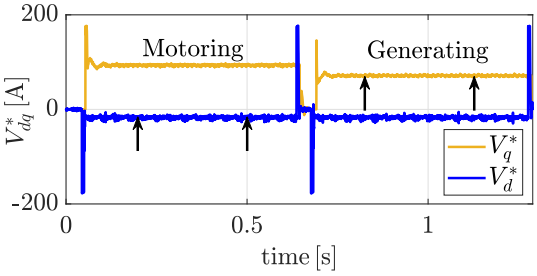

(b)

Fig. 11: Magnetic model identification test: a) dq-currents, b) dq-voltage references.

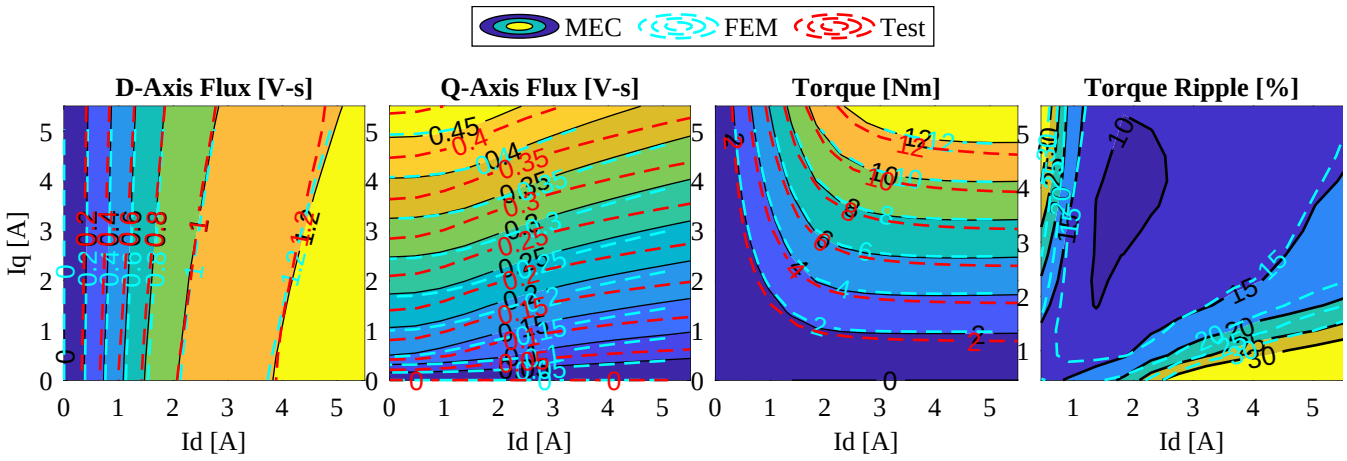

Fig. 12: Comparison of analsis results obtained with MEC and FEM.

obtained for each desired d and q-axis current, the torque can be simply calculated as:

$$T = \frac{3}{2}\, p\, (\lambda_d\, i_q - \lambda_q\, i_d) \tag{26}$$

B. Results

Due to high complexity of the machine geometry (4 rotor flux barriers and 36 stator slots), a total number of 6750 CEs were used to describe the geometry, 90 tangentially and 75 radially. Nevertheless, for a single operating point, the computational advantage of the DMEC does not diminish as it is 7.5 times faster than the FEA.

The experimental results along with the FE and DMEC analysis are reported in Fig. 12 in terms $d-$ and $q-$axis fluxes, average torque and torque ripple. A quick overall comparison show an excellent match between DMEC prediction and experimental measurements. As a general trend d-axis fluxes obtained through tests are well matching with both analysis. In terms of q-axis flux, the experimental values are lower than the predictions (both FEA and DMEC). This behaviour can be explained by the imperfect geometry description and the way flux paths occur in the DMEC. Notwithstanding this small discrepancy, the torque contours are well matching with each other. The last subfigure of Fig. 12 shows a good match between the FEA estimated and DMEC estimated torque ripple.

VI. Conclusion

A highly detailed computationally efficient and general purpose non-linear distributed magnetic equivalent circuit capable of analyzing different synchronous machine topologies has been presented in this paper. The full description of the building blocks of the modeling technique are given including details on the geometry discretization, boundary conditions definition, mmf sources definition and non-linear resolution method. The systematic use of a cell element made of four reluctances offers great flexilibity in terms of flux paths that can be modelled and consequentially geometries that can be rapresented. In addition, such systematic discretization of the space allows an easy implementation of rotation between components. Excitations due to windings and permanent magnets are considered using a unique loop based definition which avoid placing an mmf source within the single cell elements. A number of analyses have been performed with three different machines, i.e an SPM, a SynRel and a PMaSynRel machine in order to assess the performance of the propsed model against the state-of-the-art FEM in terms of accuracy and computation time. This assessment - carried out in a wide range of operating points - yields to very good results in terms of accuracy and showed that the DMEC is 12-20 times faster compared to the respective FEAs. An experimental test campaign of an off-the-shelf SynRel motor has been carried out fully validating the proposed modeling technique.

References

[1] E.R. Lwithwaite. Magnetic equivalent circuits for electrical machines. *Proceedings of the Institution of Electrical Engineers*, 114:1805–1809(4), 11 1967.

[2] G.R. Slemon. Equivalent circuits for transformers and machines including non-linear effects. *Proceedings of the IEE - Part IV: Institution Monographs*, 100:129–143(14), 09 1953.

[3] Vlado Ostovic. A method for evaluation of transient and steady state performance in saturated squirrel cage induction machines. *IEEE Transactions on Energy Conversion*, EC-1(3):190–197, 1986.

[4] V. Ostovic. A simplified approach to magnetic equivalent-circuit modeling of induction machines. *IEEE Transactions on Industry Applications*, 24(2):308–316, 1988.

[5] Scott D. Sudhoff, Brian T. Kuhn, Keith A. Corzine, and Brian T. Branecky. Magnetic equivalent circuit modeling of induction motors. *IEEE Transactions on Energy Conversion*, 22(2):259–270, 2007.

[6] G.R. Slemon. An equivalent circuit approach to analysis of synchronous machines with saliency and saturation. *IEEE Transactions on Energy Conversion*, 5(3):538–545, 1990.

[7] M.K. Jenkins, D. Howe, and T.S. Birch. An improved design procedure for hybrid stepper motors. *IEEE Transactions on Magnetics*, 26(5):2535–2537, 1990.

[8] Jin Hur, Sang-Baeck Yoon, Dong-Yun Hwang, and Dong-Seok Hyun. Analysis of pmlsm using three dimensional equivalent magnetic circuit network method. *IEEE Transactions on Magnetics*, 33(5):4143–4145, 1997.

[9] S. Vaez-Zadeh and A. Hassanpour Isfahani. Enhanced modeling of linear permanent-magnet synchronous motors. *IEEE Transactions on Magnetics*, 43(1):33–39, 2007.

[10] C.B. Rasmussen and E. Ritchie. A magnetic equivalent circuit approach for predicting pm motor performance. In *IAS '97. Conference Record of the 1997 IEEE Industry Applications Conference Thirty-Second IAS Annual Meeting*, volume 1, pages 10–17 vol.1, 1997.

[11] Yon-Do Chun, Ju Lee, and S. Wakao. Overhang effect analysis of brushless dc motor by 3-d equivalent magnetic circuit network method. *IEEE Transactions on Magnetics*, 39(3):1610–1613, 2003.

[12] M. Moallem and G.E. Dawson. An improved magnetic equivalent circuit method for predicting the characteristics of highly saturated electromagnetic devices. *IEEE Transactions on Magnetics*, 34(5):3632–3635, 1998.

[13] E.C. Lovelace, T.M. Jahns, and J.H. Lang. A saturating lumped-parameter model for an interior pm synchronous machine. *IEEE Transactions on Industry Applications*, 38(3):645–650, 2002.

[14] Y. Kano, T. Kosaka, and N. Matsui. Simple nonlinear magnetic analysis for interior permanent magnet synchronous motors. In *Second International Conference on Power Electronics, Machines and Drives (PEMD 2004).*, volume 2, pages 781–786 Vol.2, 2004.

[15] Seok-Hee Han, Thomas M. Jahns, and Wen L. Soong. A magnetic circuit model for an ipm synchronous machine incorporating moving airgap and cross-coupled saturation effects. In *2007 IEEE International Electric Machines & Drives Conference*, volume 1, pages 21–26, 2007.

[16] Z.Q. Zhu, Y. Pang, D. Howe, S. Iwasaki, R. Deodhar, and A. Pride. Analysis of electromagnetic performance of flux-switching permanent-magnet machines by nonlinear adaptive lumped parameter magnetic circuit model. *IEEE Transactions on Magnetics*, 41(11):4277–4287, 2005.

[17] Yoshiaki Kano, Kazuki Tonogi, Takashi Kosaka, and Nobuyuki Matsui. Optimization of axial-flux pm machines for improved torque density by simple non-linear magnetic analysis. In *2007 IEEE International Electric Machines Drives Conference*, volume 1, pages 27–33, 2007.

[18] Alfredo Vagati, Barbara Boazzo, Paolo Guglielmi, and Gianmario Pellegrino. Design of ferrite-assisted synchronous reluctance machines robust toward demagnetization. *IEEE Transactions on Industry Applications*, 50(3):1768–1779, 2014.

[19] Gianvito Gallicchio, Francesco Cupertino, Mauro Di Nardo, Michele Degano, and Chris Gerada. Hybrid fe-analytical procedure for fast flux map computation of permanent magnets assisted synchronous reluctance machines. In *2023 IEEE International Electric Machines 'I& Drives Conference (IEMDC)*, pages 1–7, 2023.

[20] Hanafy Mahmoud, Nicola Bianchi, Giacomo Bacco, and Nicola Chiodetto. Nonlinear analytical computation of the magnetic field in reluctance synchronous machines. *IEEE Transactions on Industry Applications*, 53(6):5373–5382, 2017.

[21] C. Bruzzese, D. Zito, and A. Tessarolo. Finite reluctance approach: A systematic method for the construction of magnetic network-based dynamic models of electrical machines. In *2014 AEIT Annual Conference - From Research to Industry: The Need for a More Effective Technology Transfer (AEIT)*, pages 1–6, 2014.

[22] Ahmed Hemeida, Antti Lehikoinen, Paavo Rasilo, Hendrik Vansompel, Anouar Belahcen, Antero Arkkio, and Peter Sergeant. A simple and efficient quasi-3d magnetic equivalent circuit for surface axial flux permanent magnet synchronous machines. *IEEE Transactions on Industrial Electronics*, 66(11):8318–8333, 2019.

[23] Gayan Watthewaduge, Ehab Sayed, Ali Emadi, and Berker Bilgin. Reluctance mesh-based modeling of switched reluctance machines. In *2021 IEEE Transportation Electrification Conference Expo (ITEC)*, pages 407–412, 2021.

[24] Shuo Yang, Yacine Amara, Wei Hua, and Georges Barakat. Development of a generic framework for lumped parameter modeling. *Open Physics*, 18(1):365–373, 2020.

[25] André M. Silva, Carlos Henggeler Antunes, André M. S. Mendes, and Fernando J. T. E. Ferreira. Generalized reluctance network framework for fast electromagnetic analysis of radial-flux machines. *IEEE Transactions on Energy Conversion*, 38(1):310–320, 2023.

[26] Oğuz Korman, Mauro Di Nardo, Mukhammed Murataliyev, Michele Degano, and Christopher Gerada. Magnetic equivalent circuit modelling of synchronous machines. In *2023 IEEE International Electric Machines & Drives Conference (IEMDC)*, pages 1–7, 2023.

[27] Reza Rajabi Moghaddam. *Synchronous Reluctance Machine (SynRM) in Variable Speed Drives (VSD) Applications*. PhD thesis, KTH, Electrical Machines and Power Electronics, 2011. QC 20110518.

[28] Oğuz Korman, Mauro Di Nardo, Michele Degano, and Chris Gerada. A novel flux barrier parametrization for synchronous reluctance machines. *IEEE Transactions on Energy Conversion*, 37(1):675–684, 2022.

[29] A. Galassini, G. Lo Calzo, A. Formentini, C. Gerada, P. Zanchetta, and A. Costabeber. ucube: Control platform for power electronics. In *2017 IEEE Workshop on Electrical Machines Design, Control and Diagnosis (WEMDCD)*, pages 216–221, 2017.

[30] Eric Armando, Radu Iustin Bojoi, Paolo Guglielmi, Gianmario Pellegrino, and Michele Pastorelli. Experimental identification of the magnetic model of synchronous machines. *IEEE Transactions on Industry Applications*, 49(5):2116–2125, 2013.

Oğuz Korman received the M.Sc. in electrical engineering from Istanbul Technical University, Turkey in 2018 and the Ph.D. degree focusing on electrical machines in 2024 from University of Nottingham, UK. He was working as an electromagnetic design engineer in A Group R&D Centre from 2017 to 2019 where he worked on design and testing of electric motors for various applications. He is currently a research fellow with the Power Electronics, Machines and Control (PEMC) Research Group within the University of Nottingham. His research interests include analysis, design and modelling of high-performance electrical machines for traction, aerospace and industrial sectors.

Mauro Di Nardo (M'18) received the M.Sc. (Hons.) degree in electrical engineering from the Polytechnic University of Bari, Italy, in 2012, and the Ph.D. degree in electrical machine design from the University of Nottingham, U.K., in 2017. From 2017 to 2019, he was with the AROL spa leading the R&D team within the Polytechnic University of Bari focusing on electrical drives design for mechatronics applications. Since the 2019, he was with the Power Electronics and Machine Control Group of the University of Nottingham as Research Fellow and from 2022 as Senior Researcher working on wide variety of projects. Since Sept-2023 he is an assistant professor in electrical machine and drives at the Polytechnic University of Bari, Italy. His research interests include the analysis, modelling, design optimizations and experimental characterization of permanent magnet and synchronous reluctance machines for automotive, aerospace and household sectors, induction motor for industrial applications as well as niche machine topologies such as bearingless and hysteresis motor. He serves as an Associate Editor for the IEEE Open Journal of Industry Applications.

Jacopo Riccio (Member, IEEE) received the B.Sc. and M.Sc. degrees in mechanical engineering from the University of Roma Tre, Rome, Italy, in 2014 and 2018, respectively, and the Ph.D. degree in electrical engineering from the University of Nottingham, Nottingham, U.K., in 2023,Since 2023, he has been a Research Fellow with the Power Electronics, Machine and Control Group, University of Nottingham. His research interests include the control of electric drives based on model-based predictive control and sensorless algorithms, and experimental characterizations of internal permanent magnet and synchronous reluctance machines for automotive and aerospace applications.

Mukhammed Murataliyev Mukhammed Murataliyev (Member, IEEE) received his Master's degree in electrical engineering from the University of Nottingham, Malaysia, in 2016. He obtained his Ph.D. degree from the University of Nottingham, in 2021, with a focus on novel synchronous reluctance motor design and optimization methods. From 2018 to 2020, he was a Researcher with the Key Laboratory of More Electric Aircraft Technology of Zhejiang Province, China. Since 2021, Dr. Murataliyev has been with the Power Electronics and Machine Control Group at the University of Nottingham, UK, initially as a Research Fellow. In 2023, he was promoted to Senior Research Fellow. His main research interests include the design and modelling of reluctance and permanent magnet machines for industrial and aerospace applications. In addition to his research roles, he currently works as a Lead Electromagnetic Design Engineer at NDSS, DER. He has been involved in a number of technical and industrial consulting projects in the aerospace and automotive sectors, working both part-time and full-time.

Michele Degano (SM'21) received his Master's degree in Electrical Engineering from the University of Trieste, Italy, in 2011, and his Ph.D. degree in Industrial Engineering from the University of Padova, Italy, in 2015. Between 2014 and 2016, he was a research fellow at The University of Nottingham, UK, within the Power Electronics, Machines and Control (PEMC) Research Group. In 2016 he was appointed Assistant Professor within the same group, promoted Associate Professor in 2020 and full professor in 2023. His main research focuses on electrical machines and drives for industrial, automotive, railway and aerospace applications, ranging from small to large power.

Chris Gerada a (Senior Member, IEEE) received the Ph.D. degree in numerical modeling of electrical machines from the University of Nottingham, Nottingham, U.K., in 2005. He was a Researcher with the University of Nottingham, working on high-performance electrical drives and on the design and modeling of electromagnetic actuators for aerospace applications. In 2008, he became a Lecturer of electrical machines, in 2011, an Associate Professor, and in 2013, a Professor with the University of Nottingham. He has secured major industrial, European and U.K. grants, authored more than 200 papers. His main research interests include the design and modeling of high-performance electric drives and machines. He was awarded a Royal Academy of Engineering Research Chair to consolidate research in the field.